Inorganic Chemistry

Article

pubs.acs.org/IC

Ion Exchange and Structural Aging in the Layered Perovskite Phases $H_{1-x}Li_xLaTiO_4$

T. W. S. Yip and E. J. Cussen*

WestCHEM, Department of Pure and Applied Chemistry, Thomas Graham Building, University of Strathclyde, 295 Cathedral Street, Glasgow, G1 1XL Scotland

Supporting Information

ABSTRACT: Grinding together the solid acid $HLaTiO_4$ with stoichiometric quantities of lithium hydroxide monohydrate gives the solid solution $H_{1-x}Li_xLaTiO_4$. The structures of these crystalline phases have been refined against neutron powder diffraction data to show that all of these compounds crystallize in the centrosymmetric space group *P*4/*nmm*. The protons and lithium cations occupy sites between the perovskite layers; the former in hydroxide groups that hydrogen-bond to adjacent layers while Li^+ is in four-coordinate sites that bridge the perovskite slabs with a geometry intermediate between square-planar and tetrahedral. The reaction proceeds rapidly, but the unit cell size continues to evolve over the course of days with a gradual compression along the interlayer direction that can be modeled using a power law dependence reminiscent of an Ostwald ripening process. On heating, these materials undergo a mass loss because of dehydration but retain the layered Ruddlesden–Popper structure up to 480 °C before a substantial loss of crystallinity on further heating to 600 °C. Impedance spectroscopy studies of the dehydrated materials shows that Li^+ mobility in these materials is lower than the $LiLaTiO_4$ end member, possibly because of microstructural effects causing large intergrain resistance through the defective phases.

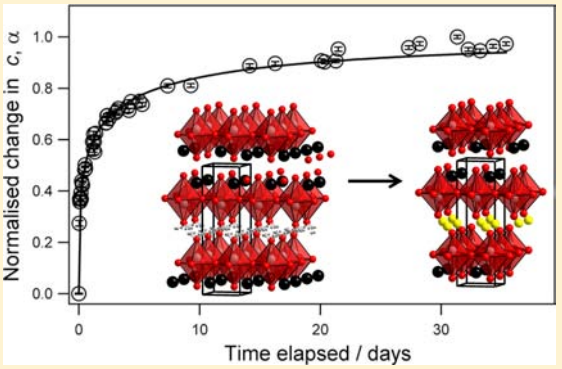

INTRODUCTION

Layered variants of the perovskite structure show many of the useful properties that are found in the parent structure combined with some of the ion-exchange reactivity of two-dimensional materials such as clays. The Ruddlesden–Popper family of compounds feature a layer of rock salt structure between the perovskite slabs and is widely studied to examine the effect of reducing dimensionality on electronic properties.[1−3] The spacing between perovskite slabs can be adjusted by replacement of the rock salt layer with other structural features[4−6] either by high-temperature synthesis or by subsequent intercalation reactions at lower temperatures. The latter rely on significant mobility of the interlayer species, and this property has been widely exploited to produce a large range of metastable compounds that are inaccessible via high-temperature syntheses.[7] Particular effort[8,9] has been made to develop phases containing Li^+ in the interlayer sites to serve as analogues for the fast Li^+ conducting perovskites $Li_{3x}La_{2/3-x}TiO_3$.[10−12] We have developed a room temperature reaction between solids that is driven by the entropy increase in releasing water from the crystal lattice of a hydrated reagent.[13] This reaction has been used to give stoichiometric control of the ion exchange of Li^+ for H^+ in the single layer Ruddlesden–Popper phase $HLaTiO_4$. In a preliminary report[14] we have shown that the reaction proceeds without dissolution of the Ruddlesden–Popper phase and that the crystallinity of the $H_{0.5}Li_{0.5}LaTiO_4$ allows identification of a random distribution of H^+ and Li^+ in the interlayer space. Here we present a detailed analysis of the structure and ion transport properties of the other compounds in the series. This includes a highly unusual aging effect that indicates movement of ions and relaxation of the structure in the interlayer region occurring over several days. Despite this mobility the total conductivity for these phases is low.

EXPERIMENTAL SECTION

The n = 1 Ruddlesden–Popper compound $NaLaTiO_4$ was prepared using conventional ceramic methods and stirred for two days in nitric acid to produce $HLaTiO_4$ as described previously.[15,16] The replacement of protons with lithium cations in $HLaTiO_4$ was carried out by grinding the solid acid with stoichiometric quantities of isotopically enriched $LiOH·H_2O$ (^7Li > 99%) under ambient conditions for 30 min as described previously.[14] This mixture was then left to stand in an open vial for about 2 days in ambient atmosphere. Multigram samples suitable for neutron powder diffraction experiments were prepared by combining several batches of lithium-exchanged product.

The structures of $HLaTiO_4$ and the lithium-exchanged phases were initially analyzed by X-ray powder diffraction using a Siemens D500 diffractometer in Bragg–Brentano geometry. These data were collected under ambient conditions using Cu K_α radiation over the

Received: February 22, 2013
Published: May 28, 2013

   dx.doi.org/10.1021/ic4004752 | *Inorg. Chem.* 2013, 52, 6985–6993

range $2 \leq 2\theta/^\circ \leq 100$. Neutron powder diffraction data were collected using the constant wavelength diffractometer D2B at the Institut Laue-Langevin, Grenoble. Samples were studied under ambient conditions and at 5 K using radiation of wavelengths 1.593 Å and 2.398 Å in the range $2 \leq 2\theta/^\circ \leq 150$.[17] Rietveld analyses of the diffraction profiles were carried out using the GSAS package,[18] and the peak shape was modeled using a pseudo-Voigt function.

X-ray powder diffraction was used to follow the progress of the reaction between $LiOH{\cdot}H_2O$ and $HLaTiO_4$ over the course of several weeks. This experiment was carried out by grinding the reagents together for about 20 min. The resulting mixture was then mounted on an X-ray diffraction sample holder, and a series of X-ray powder diffraction data sets were collected over the course of several weeks without moving the sample from the sample holder. The temperature stability of these materials was evaluated using a Perkin-Elmer TGA 7 thermal gravimetric analyzer. Because of the formation of water during the reaction, and the scope for this moisture being trapped in macropores and the possibility of decomposition via dehydration of the interlayer region, testing the temperature stability of these materials is not straightforward. Therefore the sample mass was monitored while these materials were dried at 120 °C until no further mass loss was observed at this temperature. This drying treatment was incorporated into the stability study by equilibrating samples in platinum pans at 38 °C, heating the samples to 120 °C then holding isothermally for 5 min before being heated to 800 °C at a rate of 10 °C min^{-1}. The experiments were conducted under a dynamic atmosphere of dry helium.

The transport properties of the dehydrated phases were investigated by alternating current (AC) impedance spectroscopy using a Solartron SI 1260 frequency response analyzer. These experiments were carried out by pressing approximately 0.4 g of the as-made lithium-exchanged sample under a load of 3 tonnes to give a 10 mm diameter cylindrical pellet approximately 2 mm thick. This pellet was attached to two platinum electrodes and heated from room temperature to temperatures of up to 600 °C in air. AC impedance data were then collected over the range $0.2 \leq f/Hz \leq 10^6$ on both heating and cooling the sample. Additional data were collected with the pellet contained in dynamic atmospheres of dry N_2, wet N_2 and dry O_2.

RESULTS

Structural Study. X-ray powder diffraction data collected from a sample of $HLaTiO_4$ ground with one equivalent of $LiOH{\cdot}H_2O$ showed that the layered structure of $HLaTiO_4$ had been retained, and that the lattice parameters had undergone a significant change to the values reported for $LiLaTiO_4$.[19] These observations suggest that protons had been replaced with lithium cations in a quantitative manner. Given that grinding an equimolar mixture of $HLaTiO_4$ and $LiOH{\cdot}H_2O$ appeared to result in ion exchange, this process was repeated using substoichiometric quantities of $LiOH{\cdot}H_2O$, as described by Reaction 1.

$$HLaTiO_4 + x\,^7LiOH{\cdot}H_2O \rightarrow H_{1-x}Li_xLaTiO_4 + 2xH_2O \quad \text{(Reaction 1)}$$

The samples afforded by these reactions yielded X-ray powder diffraction patterns that could be indexed using the same space group, *P*4/*nmm*, as that of both $HLaTiO_4$ and $LiLaTiO_4$ with a continuous evolution in lattice parameters between the end members that we have reported previously.[14] Here we report a full structural study of these phases using neutron diffraction to identify the structural origins for these changes in unit cell dimensions.

Neutron powder diffraction data collected from $HLaTiO_4$ were fitted using the literature model[16] in the centrosymmetric setting of the space group *P*4/*nmm*. The positions and isotropic displacement parameters of all the atoms freely refined to convergence to give the fit parameters $R_{wp} = 4.39$, $\chi^2 = 8.86$. Refining the proton occupancy gave a value of 0.119(1) that is close to the anticipated 1/8 occupancy of the 16*k* site and corresponds to a composition of $H_{0.95(1)}LaTiO_4$. Allowing partial hydrogen ordering across two different 8*l* sites in the *P*4/*n* space group resulted in an unstable refinement indicating that these data contain no evidence for proton ordering. The final structural model of $HLaTiO_4$ fixed the proton occupancy at the value of 1/8 required by charge balance and gave the fit to the data shown in Figure 1.

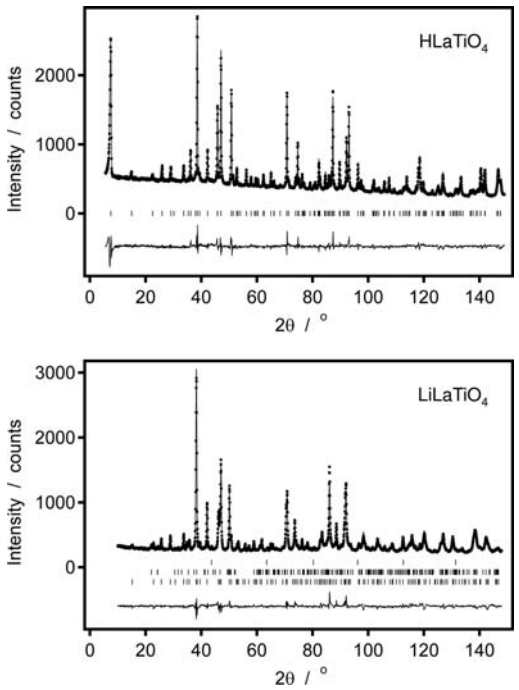

Figure 1. Observed (dots), calculated (top line), and difference (bottom line) neutron powder diffraction patterns for (a) $HLaTiO_4$ and (b) $LiLaTiO_4$ fitted in the space group *P*4/*nmm*. The vertical bars indicate the allowed Bragg reflection positions for $HLaTiO_4$. Where multiple sets of markers are shown the upper and middle markers indicate reflections allowed by vanadium and Li_2CO_3 respectively.

The neutron diffraction data collected from $LiLaTiO_4$ exhibited a highly asymmetric peak shape in the low angle (001) reflection and so this was excluded from this refinement. The data were fitted using the same model of the $[LaTiO_4]^-$ layers and employed a difference Fourier search to locate ^7Li at (1/4, 3/4, 1/2). Close inspection of the diffraction pattern revealed very weak contributions from the vanadium sample holder and a small quantity, 1.33(7) wt %, of lithium carbonate that is undetectable in the X-ray diffraction data. Both these minor phases were included in the refinement. A full refinement of this model against the neutron diffraction data was carried out using isotropic atomic displacement parameters, and resulted in the fit parameters $R_{wp} = 4.53$, $\chi^2 = 7.24$. This model provides a good fit to the observed data, as shown in Figure 1.

Neutron powder diffraction data collected from the intermediate $x = 0.5$ sample could be fitted in a similar manner to data collected from $LiLaTiO_4$, with the addition of protons on the crystallographic site identified in $HLaTiO_4$ and the H/Li content adjusted to reflect the anticipated target stoichiometry. We note that water molecules can be intercalated between the

dx.doi.org/10.1021/ic4004752 | Inorg. Chem. 2013, 52, 6985−6993

perovskite layers[15] of Ruddlesden–Popper phases with an associated expansion of the *c* lattice parameter and change in symmetry because of intercalation between alternating layers. No such water incorporation was observed in any of the compounds studied here, and there is insufficient space between the layers in the crystallographic structure. The refinement was carried out simultaneously against neutron diffraction data collected using radiation of wavelengths 1.593 Å and 2.398 Å with the asymmetric (001) reflection excluded from both data sets. The positions of all the non-hydrogen and nonlithium species as well as the isotropic displacement parameters of all the atoms readily refined to convergence to give the fit parameters R_{wp} = 4.47, χ^2 = 3.78. Similar analyses of neutron data collected at 1.593 Å from the x = 0.1, 0.25, 0.75, and 0.9 samples resulted in good agreement between the observed and calculated diffraction patterns in all cases. However, attempts to refine the hydrogen position in these H/Li-containing models led to unstable refinements, presumably because of the very low occupancy of this site. Consequently, the hydrogen was fixed at the coordinates identified in $HLaTiO_4$ with a displacement parameter constrained to a value 1.5 times larger than that of the adjacent oxide anion. For compounds containing low site occupancies of lithium, it was necessary to fix the lithium displacement parameter at a physically reasonable value of 0.012 Å^2. This value was selected from comparison with the refined values obtained from the Li-rich phases. The value chosen had minimal impact on the fit to these data sets because of the low fractional occupancy of lithium making negligible contribution to the diffraction profile.

To gauge the sensitivity of the above models to the H/Li content, the site occupancies of hydrogen (16*k* site) and lithium (2*b* site) were allowed to refine independently of each other. Unconstrained refinement of the hydrogen and lithium site occupancies of all the compounds in the series gave excellent agreement with the target stoichiometries as shown in Figure 2. The hydrogen and lithium site occupancies were

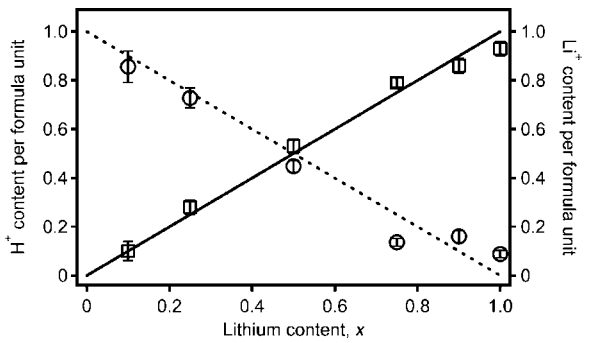

Figure 2. Hydrogen (circles) and lithium (squares) per formula unit for the $H_{1-x}Li_xLaTiO_4$ phases derived from least-squares refinement against neutron powder diffraction data. The dashed and solid lines represent the anticipated content of hydrogen and lithium respectively.

subsequently left fixed in accordance with the reaction stoichiometry, and the structures refined to convergence giving the fits shown in Figure 3. The final fit and structural parameters of all of the data sets in the series are presented in Table 1, displacement parameters are presented in Table 2, and selected bond distances and bond angles are listed in Table 3.

Ion Exchange Behavior. The rapidity of the reaction between $HLaTiO_4$ and $LiOH{\cdot}H_2O$ was assessed for an equimolar mixture of these reagents. The reagents were ground together for 20 min and underwent a temporary reduction in friability and a mass loss indicating that about 60 wt % of the water produced by Reaction 1 had been lost. X-ray powder diffraction data collected immediately after mixing the reagents for 20 min gave the pattern shown in Figure 4. This showed that the peak positions had changed substantially from those observed in $HLaTiO_4$ and resembled those of $LiLaTiO_4$ indicating that the ion exchange had occurred. However, repeating the data collection several hours later showed a small but significant change in the lattice parameters. The reaction was repeated, and diffraction patterns recorded over the following five weeks showed that the *a* lattice parameter changes rapidly while the *c* parameter evolves as a function of time as shown in Figure 4. Samples used in the neutron powder diffraction study were prepared at least one week prior to the data collection.

Normalizing the change in the *c* parameter between the initial value of $HLaTiO_4$ and the value observed after 35 days shows a power law dependence as shown in Figure 5. Fitting all of the data using eq 1

$$\alpha = 1 - \exp[(-kt)^n] \quad (1)$$

gives values of k = 0.064(3) and n = 0.332(8) and provide an excellent fit over the full range of data.

Thermal Stability. Thermogravimetric data collected from each of the samples in the $H_{1-x}Li_xLaTiO_4$ series indicate a mass loss ranging from 3.7 wt %, for $HLaTiO_4$, to 1.4 wt %, for $LiLaTiO_4$, in the temperature range $160 \leq T/°C \leq 720$. The initial mass loss on heating from room temperature is ascribed to the loss of water formed via Reaction 1 that may be in macropores on the surface. Representative data collected from $H_{0.5}Li_{0.5}LaTiO_4$ are shown in Figure 6. By representing these mass losses as the number of moles of water lost per formula unit a trend in water loss is evident suggesting that the following reaction has occurred

$$H_{1-x}Li_xLaTiO_4 \rightarrow \square_{1-x}Li_xLaTiO_{4-(1-x)/2} + \frac{1}{2}(1-x)H_2O$$

The dehydration of these lithium-exchanged phases is approximately consistent with the formula stoichiometries derived from the neutron powder diffraction study with some deviation from the anticipated mass loss arising from evaporation of extra-framework moisture.

Topotactic dehydration of the $HLaTiO_4$ parent phase can be achieved[20] by heating the material at 480 °C to form a defective n = 2 Ruddlesden–Popper phase, $La_2\square Ti_2O_7$. Applying the same heat treatment to lithium-rich members of the $H_{1-x}Li_xLaTiO_4$ series gives rise to X-ray powder diffraction patterns that can be indexed using the *P*4/*nmm* cell of the parent phase with a considerable reduction of the *c* lattice parameter. Because of peak broadening it was not possible to carry out meaningful fits to the data collected from the compounds that had shown the largest mass losses. However, the lattice parameters for the x = 0.75 and 0.9 samples could be extracted from LeBail fits to the diffraction data using the unit cell of the $[LaTiO_4]^-$ host lattice. Attempted Rietveld analyses of the structures yielded unstable refinements and so it was not possible to establish from these data that the mass loss results from dehydration of the interlayer region. Heating $LiLaTiO_4$ at 480 °C gave no significant change in cell volume indicating the

dx.doi.org/10.1021/ic4004752 | Inorg. Chem. 2013, 52, 6985–6993

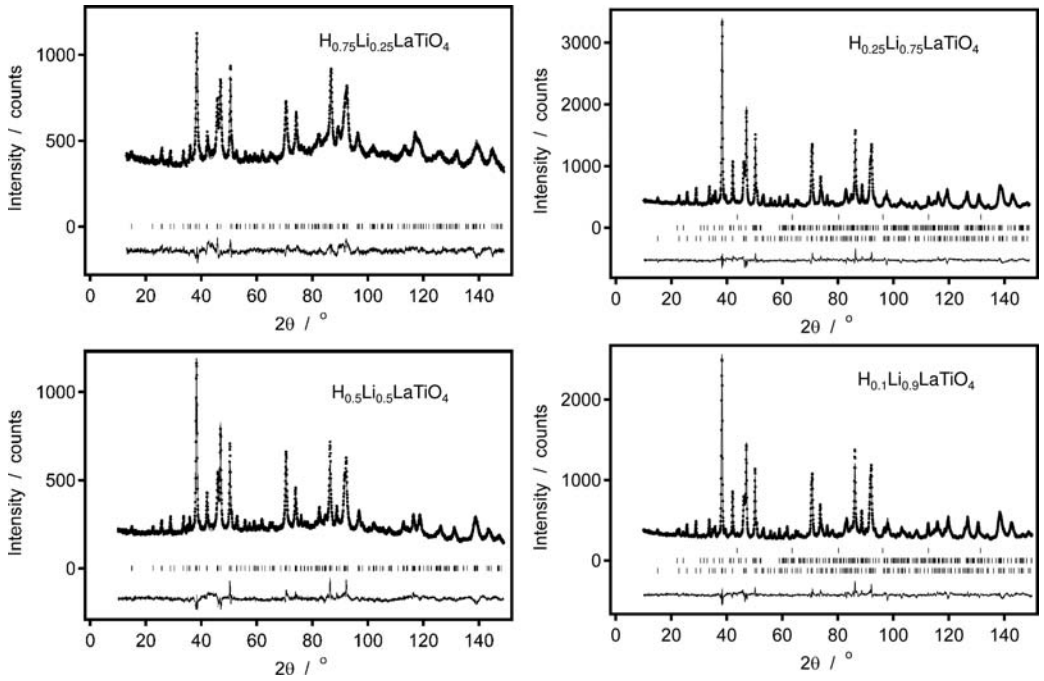

Figure 3. Observed (dots), calculated (top line), and difference (bottom line) neutron powder diffraction patterns for selected samples from the $H_{1-x}Li_xLaTiO_4$ series. The lowest vertical bars indicate the allowed Bragg reflection positions for these *P*4/*nmm* Ruddlesden−Popper phases. Where multiple sets of markers are shown the upper and middle markers indicate reflections allowed by vanadium and Li_2CO_3 respectively.

Table 1. Structural Parameters for the $H_{1-x}Li_xLaTiO_4$ Series of Compounds Derived from Least-Squares Refinement against Neutron Powder Diffraction Data Collected at Room Temperature unless Otherwise Stated[a]

compound	*a*/Å	*c*/Å	*V*/Å^3	R_{wp}	χ^2	La 2*c z*	Ti 2*c z*	O(1) 4*f z*	O(2) 2*c z*	O(3) 2*c z*
$HLaTiO_4$	3.72006(5)	12.2914(3)	170.099(6)	4.39	8.863	0.8811(2)	0.2957(4)	0.7428(2)	0.4442(3)	0.0782(2)
$H_{0.9}Li_{0.1}LaTiO_4$	3.7230(2)	12.280(2)	170.20(3)	3.42	3.553	0.8842(5)	0.3047(9)	0.7438(5)	0.4448(7)	0.0741(6)
$H_{0.75}Li_{0.25}LaTiO_4$	3.7379(2)	12.279(2)	171.56(3)	3.10	4.378	0.8822(4)	0.2981(6)	0.7451(4)	0.4410(5)	0.0799(4)
$H_{0.5}Li_{0.5}LaTiO_4$[b]	3.75083(14)	12.2161(7)	171.86(2)	4.48	3.792	0.8814(2)	0.2966(4)	0.7445(2)	0.4401(3)	0.0794(2)
$H_{0.5}Li_{0.5}LaTiO_4$ (5 K)	3.74442(13)	12.2036(7)	171.10(2)	3.83	3.991	0.8821(3)	0.2949(5)	0.7452(2)	0.4425(3)	0.0794(3)
$H_{0.25}Li_{0.75}LaTiO_4$	3.75834(9)	12.1513(5)	171.638(11)	3.59	5.970	0.8809(2)	0.2950(3)	0.7431(2)	0.4409(2)	0.0792(2)
$H_{0.1}Li_{0.9}LaTiO_4$	3.76123(9)	12.1116(5)	171.341(11)	3.97	5.815	0.8802(2)	0.2965(3)	0.7427(2)	0.4412(2)	0.0801(2)
$LiLaTiO_4$	3.76411(8)	12.0747(4)	171.081(9)	4.47	7.046	0.8802(2)	0.2978(3)	0.7425(2)	0.4414(2)	0.0799(2)

[a]Atomic coordinates: La 2*c* (1/4, 1/4, *z*), Ti 2*c* (1/4, 1/4, *z*), O(1) 4*f* (3/4, 1/4, *z*), O(2) 2*c* (1/4, 1/4, *z*), O(3) 2*c* (1/4, 1/4, *z*), H 16*k* (0.387(9), 0.068(9), 0.4869(12)), Li 2*b* (1/4, 3/4, 1/2). Atomic coordinates of protons were derived from full refinement of the $HLaTiO_4$ parent phase, and were fixed at these values for all other proton-containing phases. [b]Simultaneous refinement against 1.593 Å and 2.39766(14) Å wavelength data sets.

Table 2. Atomic Displacement Parameters, $100U_{iso}$ (Å^2), for the $H_{1-x}Li_xLaTiO_4$ Series of Compounds Derived from Least-Squares Refinement against Neutron Powder Diffraction Data

compound	H 16*k*[a]	Li 2*b*	La 2*c*	Ti 2*c*	O(1) 4*f*	O(2) 2*c*	O(3) 2*c*
$HLaTiO_4$	5.4(6)	n/a	0.72(4)	0.79(9)	0.75(4)	2.51(8)	0.75(6)
$H_{0.9}Li_{0.1}LaTiO_4$	5.6(3)	1.2	1.61(10)	3.1(3)	1.29(9)	3.8(2)	2.0(2)
$H_{0.75}Li_{0.25}LaTiO_4$	1.9(2)	1.2	0.99(9)	0.4(2)	0.57(8)	1.26(14)	0.37(11)
$H_{0.5}Li_{0.5}LaTiO_4$	2.63(13)	2.2(4)	1.23(6)	1.08(13)	0.94(5)	1.75(9)	1.12(8)
$H_{0.5}Li_{0.5}LaTiO_4$ (5 K)	2.13(15)	1.0(4)	1.18(7)	1.1(2)	0.35(5)	1.42(10)	0.34(8)
$H_{0.25}Li_{0.75}LaTiO_4$	1.63(9)	1.2(2)	0.51(4)	0.29(8)	0.36(4)	1.08(6)	0.66(6)
$H_{0.1}Li_{0.9}LaTiO_4$	1.68(9)	1.7(2)	0.41(4)	0.18(9)	0.39(4)	1.12(6)	0.64(6)
$LiLaTiO_4$	n/a	2.0(2)	0.80(4)	0.28(8)	0.69(4)	1.06(5)	1.04(6)

[a]Constrained atomic displacement parameter: U_{iso} H = 1.5 × U_{iso} O(2)

mass loss observed for this sample in thermogravimetric measurements arises from evaporation of extra-framework moisture.

Heating the dehydrated samples to 600 °C leads to minimal further mass loss but resulted in a considerable loss of crystallinity. The materials formed on heat treatment at 600 °C shall be referred to as $\square_{1-x}Li_xLaTiO_{4-(1-x)/2}$ (HT).

Ionic Conductivity. Impedance data were collected from the two high-temperature samples $\square_{0.5}Li_{0.5}LaTiO_{3.75}$ (HT) and $\square_{0.25}Li_{0.75}LaTiO_{3.875}$ (HT) and also from a sample of $\square_{0.25}Li_{0.75}LaTiO_{3.875}$ after heating to 480 °C. In each case the

dx.doi.org/10.1021/ic4004752 | *Inorg. Chem.* 2013, 52, 6985−6993

Table 3. Selected Bond Distances (Å) and Angles for $H_{1-x}Li_xLaTiO_4$ Derived from Least-Squares Refinement against Neutron Powder Diffraction Data Collected at Room Temperature

compound	H–O2[a] ×8	H–O2[b] ×8	Li–O(2)×4	La–O(1)×4	La–O(3)	La–O(3)×4	Ti–O(1)×4	Ti–O(2)	Ti–O(3)	O(1)–Ti–O(1)	O(1)–Ti–O(2)	$O(2)_z$···$O(2)_z$
$HLaTiO_4$	0.997(14)	1.984(13)	n/a	2.519(2)	2.423(3)	2.6778(7)	1.9195(12)	1.825(6)	2.674(5)	86.50(6)	104.3(1)	1.372(7)
$H_{0.9}Li_{0.1}LaTiO_4$	0.993(5)	1.983(4)	1.981(3)	2.537(5)	2.332(9)	2.682(2)	1.955(4)	1.72(2)	2.83(2)	84.7(2)	107.8(3)	1.36(2)
$H_{0.75}Li_{0.25}LaTiO_4$	1.021(3)	2.009(3)	2.005(2)	2.515(4)	2.427(6)	2.6839(14)	1.943(2)	1.755(11)	2.679(9)	85.72(12)	105.8(2)	1.449(13)
$H_{0.5}Li_{0.5}LaTiO_4$	1.023(2)	2.018(2)	2.0131(13)	2.513(2)	2.419(4)	2.6949(7)	1.9416(13)	1.753(6)	2.653(5)	86.16(7)	105.0(1)	1.463(7)
$H_{0.25}Li_{0.75}LaTiO_4$	1.022(2)	2.0146(11)	2.0115(9)	2.517(2)	2.409(3)	2.7015(5)	1.9353(10)	1.774(5)	2.622(4)	86.72(6)	103.8(1)	1.436(5)
$H_{0.1}Li_{0.9}LaTiO_4$	1.020(2)	2.0132(12)	2.011(1))	2.512(2)	2.421(3)	2.7028(5)	1.9397(11)	1.753(5)	2.621(5)	86.56(6)	104.2(1)	1.424(5)
$LiLaTiO_4$	n/a	n/a	2.0108(9)	2.511(2)	2.412(3)	2.7049(5)	1.9439(11)	1.733(5)	2.631(5)	86.41(6)	104.5(1)	1.415(5)

[a]Proton-oxide separation immediately about the apical oxide position, i.e., a hydroxyl group. [b]Proton-oxide separation that spans the interlayer region, i.e., a hydrogen bond.

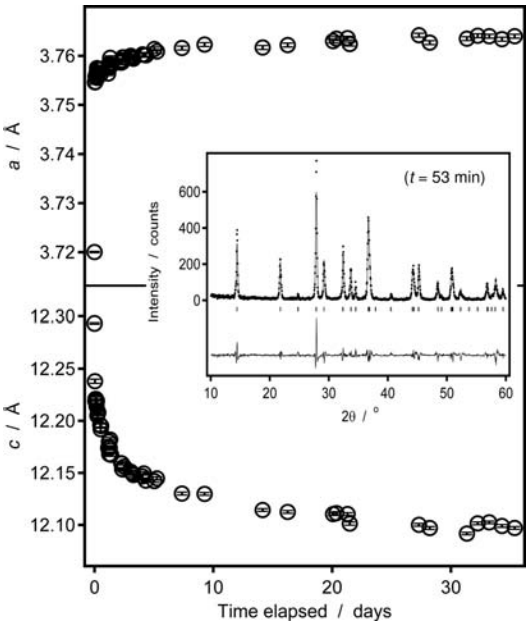

Figure 4. Evolution in lattice parameters for $H_{0.5}Li_{0.5}LaTiO_4$ as a function of time after initiating the reaction between $LiOH{\cdot}H_2O$ and $HLaTiO_4$. The error bars indicate one standard deviation derived from Rietveld refinement against each of the X-ray diffraction patterns. The inset shows the pattern resulting from a 30 min X-ray diffraction data collection that was performed immediately after mixing the reagents for 20 min and fitted using Rietveld refinement.

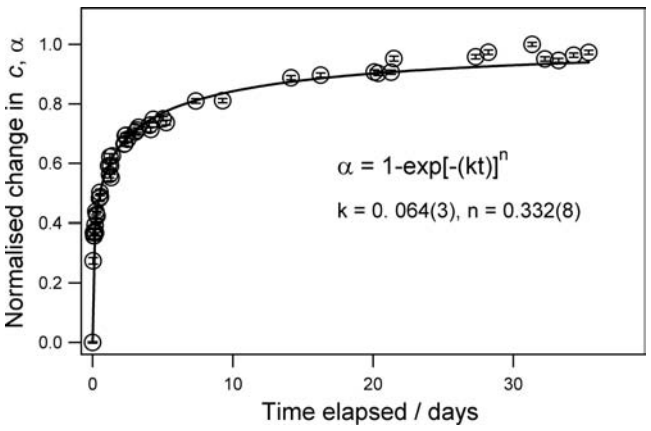

Figure 5. Change in the *c* lattice parameter showed a power law dependence on $time^{1/3}$. The error bars correspond to one standard deviation in the normalized *c* lattice parameter.

data showed multiple overlapping arcs in the complex plane that could not be deconvoluted to extract information on inter- or intragrain ionic conductivity. An estimate of the total conductivity was made by addition of the resistances from multiple combinations of resistor and constant phase element in parallel. The most conducting sample, $\square_{0.25}Li_{0.75}LaTiO_{3.875}$ (HT), showed a low frequency tail as shown in Figure 7 indicating that the electrodes are blocking the passage of charged species. Arrhenius analyses of the resultant total conductivities as shown in Figure 7 gave conductivities of around 10^{-7} S cm^{-1} with activation energies in the range 0.8 to 0.9 eV. The measurements on $\square_{0.5}Li_{0.5}LaTiO_{3.75}$ (HT) were repeated in dry and wet atmospheres of N_2 and O_2, and the impedance was unaffected by changes in the partial pressure of either water or oxygen as shown in Figure 8.

dx.doi.org/10.1021/ic4004752 | Inorg. Chem. 2013, 52, 6985−6993

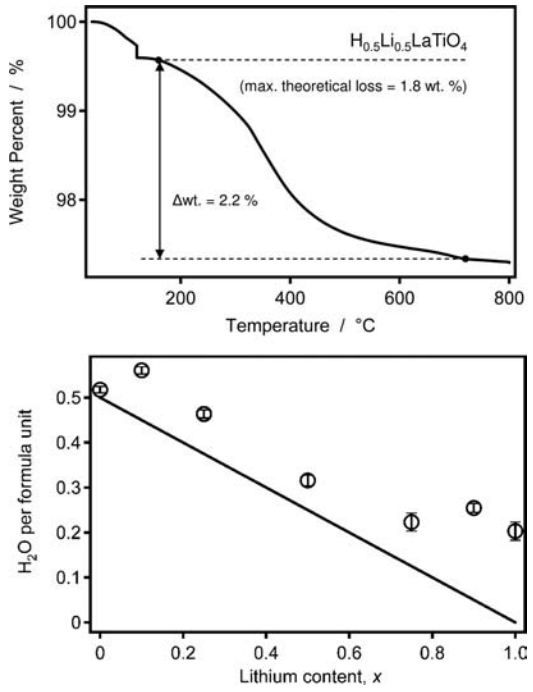

Figure 6. (a) Change in mass on heating $H_{0.5}Li_{0.5}LaTiO_4$ from room temperature to 800 °C under a dynamic atmosphere of dry helium. The limits of the mass loss, Δwt., are defined by a significant change in gradient on heating above 120 °C and approaching 800 °C. The maximum loss in mass anticipated from the topochemical dehydration of $H_{0.5}Li_{0.5}LaTiO_4$ is 1.8 wt %. The mass change derived from the TGA data is expressed as loss of water molecules per formula unit in (b). The solid line represents the losses of water anticipated from the topochemical dehydration reaction.

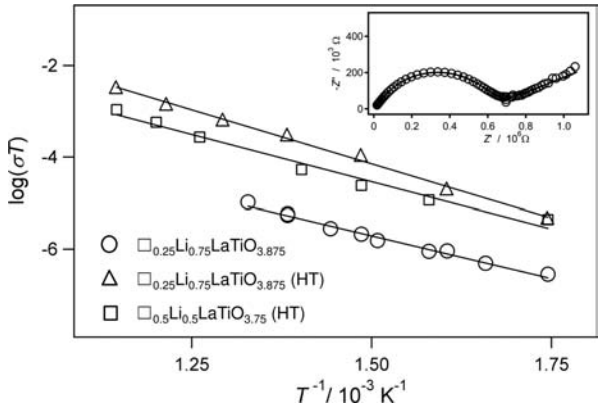

Figure 7. Arrhenius plots of conductivity as a function of temperature for $\square_{0.5}Li_{0.5}LaTiO_{3.75}$ (HT) (squares), $\square_{0.25}Li_{0.75}LaTiO_{3.875}$ (circles), and $\square_{0.25}Li_{0.75}LaTiO_{3.875}$ (HT) (triangles), on heating. These conductivities were derived from AC impedance data collected in air. The solid lines indicate the least-squares fit to each data set that was used to derive the activation energy for conduction. The inset shows a complex plane plot of the impedance of $\square_{0.25}Li_{0.75}LaTiO_{3.875}$ (HT) at 450 °C.

DISCUSSION

The room-temperature mixing of crystalline $LiOH{\cdot}H_2O$ with the layered perovskite $HLaTiO_4$ initiates an ion-exchange reaction, where protons are quantitatively replaced with lithium cations to give the continuous solid-solution $H_{1-x}Li_xLaTiO_4$. This direct room-temperature approach can be contrasted with

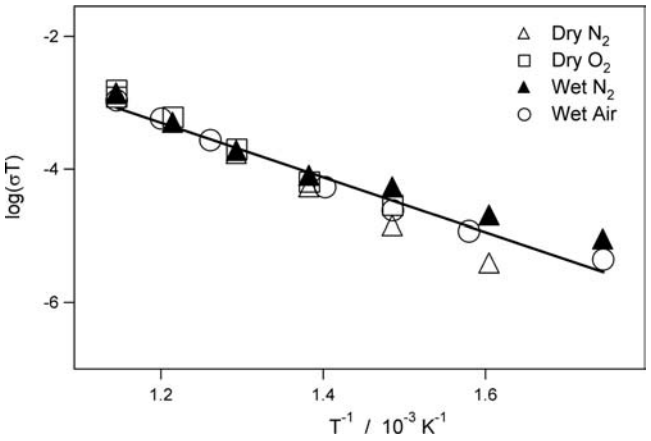

Figure 8. Arrhenius plots of conductivity as a function of temperature for $\square_{0.5}Li_{0.5}LaTiO_{3.75}$ (HT) derived from AC impedance data collected in air (circles), dry oxygen (squares), dry nitrogen (triangles), and wet nitrogen (filled triangles). The solid lines indicate the least-squares fit corresponding to an activation energy of 0.8 eV.

other methods of ion exchange for layered materials,[7] which often employ an excess of cations in either aqueous solution[19] or molten salt[15,21] to drive the exchange. These typically lead to the fully exchanged material although the double-layer phase $HLiSrTa_2O_7$ has recently been prepared by careful control of the quantity and concentration of acid used to drive the partial replacement of Li^+ with H^+.[22] Here we have instead exploited the gain in entropy associated with the liberation of water from the lattice[13] of $LiOH{\cdot}H_2O$ to drive the exchange of a controlled quantity of lithium cations in an acid–base reaction to give stoichiometric control over the degree of ion exchange. We have previously shown that the products of these reactions retain the morphology of the $HLaTiO_4$ reagent,[14] and this suggests that the water liberated during the reaction does not dissolve the Ruddlesden–Popper phase. This can be contrasted with the reaction between $LiOH{\cdot}H_2O$ and MoO_3 to form Li_2MoO_4 that involves dissolution and does not proceed when anhydrous LiOH is mixed with MoO_3 showing that the water of crystallization plays a vital role in the reaction.[13] This reaction can occur in dry air and so contrasts with the reaction between $LiOH{\cdot}H_2O$ and $Al(OH)_3$ that requires the presence of atmospheric moisture to give the hydrated phase $[LiAl_2(OH)_6]^+OH^-{\cdot}2H_2O$.[23]

The structures of the partially exchanged phases are very similar to those of the $HLaTiO_4$ and $LiLaTiO_4$ end members; both the staggering of adjacent perovskite layers and the ordered arrangement of La^{3+} and H^+/Li^+ cations are maintained throughout the series. The coordination environments adopted by hydrogen and lithium are also largely constant for all compounds as illustrated in Figure 9. In $HLaTiO_4$, protons are statistically distributed over eight equivalent sites about the apical oxide position, O(2), at a distance of 0.997(14) Å that is typical for hydroxide.[24] A longer proton-oxide separation of 1.984(13) Å that spans the interlayer region with an O(2)–H···O(2) angle of 116.8° is typical of hydrogen-bond geometry.[25] The relatively large atomic displacement parameters of O(2) suggest that the oxide is displaced by the presence of the proton. This interpretation is supported by the neutron power diffraction study of $H_{0.5}Li_{0.5}LaTiO_4$, conducted at 5 K; the atomic displacement parameters of the oxide anions within the perovskite plane and projecting toward the La^{3+} cations decrease to one-third of their room-temperature values, while

dx.doi.org/10.1021/ic4004752 | Inorg. Chem. 2013, 52, 6985–6993

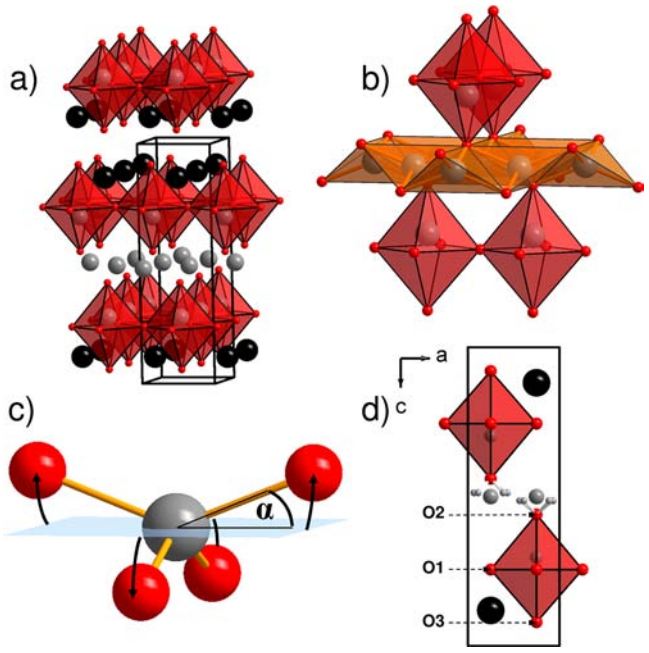

Figure 9. (a) Layered structure of $LiLaTiO_4$ contains Li^+ cations, shown in gray, between the layers of TiO_6 represented by octahedra. (b) The Li^+ cations link adjacent layers via four coordination in a geometry intermediate between square planar and tetrahedral as defined in (c) by the angle α. The three crystallographically distinct oxide ions are labeled in (d), and the disordered hydrogen atoms are illustrated as small gray spheres that are bonded to O(2) to form hydroxide groups.

the O(2) anion projecting toward H/Li in the rock salt layer shows a larger degree of disorder.

The lithium cations in $LiLaTiO_4$ provide a robust link between the perovskite layers by bonding to two oxide anions from each layer to give four equal Li−O bond lengths of 2.0108(9) Å. These LiO_4 units form O−Li−O angles of about 139° and 97° as shown in Figure 9. This unusual distortion is characteristic of a number of lithium-containing layered perovskite phases[26] although it should be noted that in only some of these cases have the lithium cations been explicitly located by neutron powder diffraction.[22,27] The size of distortion of square planar coordination toward a tetrahedral arrangement can be quantified using the angle, α, between the *xy* plane and a Li−O bond that varies from 0° for a square planar to 35.26° for a regular tetrahedral coordination. In these materials this angle is almost invariant with composition at 21.0(4)°. This can be expressed using eq 2[28] to reveal a largely constant value for the distortion, $\varphi(T\text{-}SP)$, of 41(1) % square planarity for the LiO_4 units across the series of compositions.

$$\varphi(T - SP) = \left(1 - \frac{\alpha}{35.26°}\right) \times 100 \qquad (2)$$

The replacement of protons with lithium cations results in a reduction in the *c* lattice parameter, despite the ionic radius of Li^+ being larger than that of H^+. In the case of full-exchange to give $LiLaTiO_4$, this decreases *c* by 0.2167(5) Å compared to $HLaTiO_4$. The introduction of Li^+ actually increases the interlayer separation by about 0.06 Å, and the overall reduction in *c* arises from more substantial changes in the perovskite layers in response to lithium intercalation. As the lithium content is increased the TiO_6 octahedra undergo a compression along the *z* direction with the O(2)−Ti-O(3) distance shortened by up to 0.135(11) Å compared to $HLaTiO_4$ as shown in Figure 9. This reduction in the apical Ti−O bond lengths is accompanied by an extension of the equatorial bonds in these octahedral units in such a manner that the bond valence is maintained; the calculated valences of Ti of 4.09(3) and 4.18(3) in $HLaTiO_4$ and $LiLaTiO_4$ respectively are as expected for Ti^{4+}.[29]

The Li−O bond distance shows no significant variation across the series, with a typical value of 2.0108(9) Å indicated by the $LiLaTiO_4$ end member. A bond valence sum analysis of this distance indicates a valence of 0.916(4), suggesting that the distorted tetrahedral site of lithium is slightly larger than the optimum size. It is interesting to note that the calculation of the bond valence for a hypothetical Li^+ placed on the vacant 2*b* site of $HLaTiO_4$ resulted in a valence of 0.992(4) indicating that this site provides a better match to a typical Li−O environment. An analysis of lithium coordination environments in related $n = 2$ Ruddlesden−Popper structures gave similarly low values of 0.81(2) for $Li_2La_{2/3}Ta_2O_7$,[9] 0.792(2) for $Li_2SrTa_2O_7$,[27] and values of 0.64(2) and 0.82(4) for the two Li^+ sites in $HLiSrTa_2O_7$.[22] This suggests that there is a tendency for lithium to be under-bonded in Ruddlesden−Popper structures.

It has previously been shown[14] that the samples produced by these ion-exchange reactions have the same particle morphology as the $HLaTiO_4$ parent strongly suggesting that protons had been replaced by lithium cations without dissolution or delamination of the Ruddlesden−Popper lattice.[30] These observations are supported by X-ray powder diffraction data collected from an equimolar mixture of the reagents over the course of several weeks. This study indicates the presence of a single phase that is crystalline and shows a time-evolved change in the lattice parameters rather than a transition via an amorphous intermediate.

The ion-exchange reaction is most readily detected in the change in the lattice parameters although the structure shows anisotropic rates of change for the formation of $LiLaTiO_4$ from $HLaTiO_4$; the *a* parameter undergoes 75% of the total expansion within 50 min of mixing the reagents while the *c* parameter changes at a slower rate and takes 12 h to undergo 50% of the contraction. This relatively slow contraction of the structure along the interlayer direction indicates that some degree of structural rearrangement is occurring over the course of several days following the reaction. These differential rates of change of the lattice parameters result from the difference between the structural effects that drive the changes within the *ab* plane compared to those controlling the behavior perpendicular to this. The rapid expansion along *a* results from the lengthening of equatorial Ti−O bonds in response to bonding of Li^+ to the apical oxide anions as discussed above.

While changes in *a* depend on local bonding interactions, the changes in *c* are more complex. If the perovskite layers are considered as parallel, rigid sheets then the intercalation of a single ion could be anticipated to lead to a large expansion of *c* while a corresponding reduction would require the removal of *all* intercalated species. The observed slow contraction of *c* could be indicative of either the ongoing elimination of H^+ from the material or it may reflect a subsequent relaxation of the Li^+ cations to the optimum coordination environments identified by neutron diffraction. Describing the time dependence of *c* using a power law shows a $t^{1/3}$ relationship that is reminiscent of Ostwald ripening of three-dimensional particles.[31] This may reflect an increase in the domain size for Li^+

dx.doi.org/10.1021/ic4004752 | *Inorg. Chem.* 2013, 52, 6985−6993

order within the structure with time. However, the layered nature of the structure suggests that ion migration could be constrained to two-dimensions and so this similarity with unconstrained particle growth may be fortuitous.[32]

Heating these materials to 480 °C gives a substantial reduction in mass because of the formation of water by the protons and apical oxide anions in the interlayer region and subsequent loss of this water from the structure. The X-ray powder diffraction study of the resultant dehydrated materials indicates that the basic structure of the Ruddlesden−Popper phase is retained, presumably as a consequence of Li−O bonds bridging between the perovskite layers. It is important to note that a lithium cation in the interlayer region with a coordination number of greater than two will always lead to bridging of the defective perovskite layers. Therefore, it is likely that the layers will remain more rigidly held together in the lithium-rich samples. This is supported by the observation that the dehydration of $H_{0.5}Li_{0.5}LaTiO_4$ was accompanied by a considerable loss of crystallinity that was not apparent for the lithium-rich phases.

The observations accumulated from both the X-ray and the TGA experiments show that the lithium-exchanged phases over the range $0.5 \leq x \leq 0.9$ lose water, but retain a structure and composition that can probably be described as $\square_{1-x}Li_xLaTiO_{4-(1-x)/2}$.

Although the structures of these dehydrated phases are not well understood, they presumably contain a mixture of occupied and vacant lithium sites, and thus bear strong similarities to the fast lithium-conducting perovskites $Li_{3x}La_{2/3-x}TiO_3$.[10,12] Despite these similarities, the transport measurements of $\square_{0.25}Li_{0.75}LaTiO_{3.875}$ indicated that the total conductivity of this material (ca. 8.0×10^{-9} S cm^{-1} at 450 °C) is many orders of magnitude lower than that of $Li_{3x}La_{2/3-x}TiO_3$ (ca. 10^{-3} S cm^{-1} at 25 °C).[33] The conductivity is unaffected by changes in partial pressure of either oxygen or water, and this indicates that the ionic charge transport is occurring via mobility of Li^+ rather than movement of H^+ or O^{2-}.

The $LiLaTiO_4$ end member has a total conductivity of about 3×10^{-6} S cm^{-1} at 450 °C[34] that is at least 2 orders of magnitude higher than that of $\square_{0.25}Li_{0.75}LaTiO_{3.875}$. Given the similarity in structures and compositions it would be expected that the material with vacant lithium sites would show a higher intragrain conductivity. Our impedance data were only able to provide an estimate of the total conductivity, and it appears that the considerable difference in conductivity arises from a dominant grain boundary contribution to the total resistance. The X-ray powder diffraction data collected from the dehydrated samples show peak broadening that is indicative of microstructural changes in the sample, and it is likely that this increase in grain boundary concentration is responsible for the reduction in Li^+ mobility through the material.

CONCLUSIONS

The Ruddlesden−Popper phases $H_{1-x}Li_xLaTiO_4$ form an isostructural series with an arrangement of interlayer H^+ and Li^+ that is disordered on the diffraction length scale. Protons form hydroxyl groups with the oxide anions that project out of the perovskite layer while Li^+ is present in a four-coordinate environment that is intermediate between square planar and tetrahedral geometry. These materials form within minutes of commencing the room temperature reaction, but show a gradual compression along the interlayer direction that follows a 1/3 power law. This clearly indicates that the ions display some local mobility at room temperature that can be detected over diffraction length scales. However, bulk ionic conductivity through the material remains low in both the as-prepared materials and those which have undergone dehydration to generate Ruddlesden−Popper structures with considerable disorder and some loss of crystallinity.

ASSOCIATED CONTENT

Supporting Information

Additional X-ray powder diffraction patterns collected after heating samples at 480 and 600 °C. This material is available free of charge via the Internet at http://pubs.acs.org.

AUTHOR INFORMATION

Corresponding Author

*E-mail: Edmund.Cussen@Strath.ac.uk. Phone: +44 141 548 2797. Fax: +44 141 548 4822.

Notes

The authors declare no competing financial interest.

ACKNOWLEDGMENTS

The authors are grateful to the Royal Society for the provision of a University Research Fellowship to E.J.C. and to the University of Strathclyde for funding and to Dr. Emmanual Suard at the Institut Laue-Langevin for assistance with neutron diffraction experiments.

REFERENCES

(1) Kimura, T.; Tomioka, Y.; Kuwahara, H.; Asamitsu, A.; Tamura, M.; Tokura, Y. *Science* **1996**, *274*, 1698.
(2) Battle, P. D.; Bell, A. M. T.; Blundell, S. J.; Coldea, A. I.; Cussen, E. J.; Hardy, G. C.; Marshall, I. M.; Rosseinsky, M. J.; Steer, C. A. *J. Am. Chem. Soc.* **2001**, *123*, 7610.
(3) Cussen, E. J.; Thomas, M. F. *J. Mater. Chem.* **2005**, *15*, 1084.
(4) Liang, Z.; Tang, K.; Zeng, S.; Wang, D.; Li, T.; Zheng, H. *J. Solid State Chem.* **2008**, *181*, 2565.
(5) McCabe, E. E.; Jones, I. P.; Zhang, D.; Hyatt, N. C.; Greaves, C. *J. Mater. Chem.* **2007**, *17*, 1193.
(6) Sivakumar, T.; Seshadri, R.; Gopalakrishnan, J. *J. Am. Chem. Soc.* **2001**, *123*, 11496.
(7) Schaak, R. E.; Mallouk, T. E. *Chem. Mater.* **2002**, *14*, 1455.
(8) Thangadurai, V.; Shukla, A. K.; Gopalakrishnan, J. *Chem. Mater.* **1999**, *11*, 835.
(9) Le Berre, F.; Crosnier-Lopez, M.-P.; Laligant, Y.; Suard, E.; Bohnke, O.; Emery, J.; Fourquet, J.-L. *J. Mater. Chem.* **2004**, *14*, 3558.
(10) Alonso, J. A.; Sanz, J.; Santamaria, J.; Leon, C.; Varez, A.; Fernandez-Diaz, M. T. *Angew. Chem., Int. Ed.* **2000**, *39*, 619.
(11) Stramare, S.; Thangadurai, V.; Weppner, W. *Chem. Mater.* **2003**, *15*, 3974.
(12) Yashima, M.; Itoh, M.; Inaguma, Y.; Morii, Y. *J. Am. Chem. Soc.* **2005**, *127*, 3491.
(13) Yip, T. W. S.; Cussen, E. J.; Wilson, C. *Dalton Trans.* **2010**, *39*, 411.
(14) Yip, T. W. S.; Cussen, E. J.; MacLaren, D. A. *Chem. Commun.* **2010**, *46*, 698.
(15) Byeon, S.-H.; Yoon, J.-J.; Lee, S.-O. *J. Solid State Chem.* **1996**, *127*, 119.
(16) Nishimoto, S.; Matsuda, M.; Harjo, S.; Hoshikawa, A.; Kamiyama, T.; Ishigaki, T.; Miyake, M. *J. Eur. Ceram. Soc.* **2006**, *26*, 725.
(17) Hewat, A. W. *Phys. B: Condens. Matter* **2006**, *385−86*, 979.
(18) Larson, A. C.; ; von Dreele, R. B. *General Structure Analysis System (GSAS)*; Los Alamos National Laboratories: Los Alamos, NM, 1990.
(19) Toda, K.; Kurita, S.; Sato, M. *J. Ceram. Soc. Jpn.* **1996**, *104*, 140.

(20) Thangadurai, V.; Subbanna, G. N.; Gopalakrishnan, J. *Chem. Commun.* **1998**, 1299.
(21) Neiner, D.; Spinu, L.; Golub, V.; Wiley, J. B. *Chem. Mater.* **2006**, *18*, 518.
(22) Galven, C.; Fourquet, J. L.; Suard, E.; Crosnier-Lopez, M. P.; Le Berre, F. *Dalton Trans.* **2010**, *39*, 3212.
(23) Poeppelmeier, K. R.; Hwu, S.-J. *Inorg. Chem.* **1987**, *26*, 3297.
(24) Ferraris, G.; Ivaldi, G. *Acta Crystallogr.* **1984**, *B40*, 1.
(25) Brown, I. D. *Acta Crystallogr.* **1975**, *A32*, 24.
(26) Mitchell, R. H. *Perovskites: Modern and Ancient*; Almaz Press: Thunder Bay, Ontario, Canada, 2002.
(27) Pagnier, T.; Rosman, N.; Galven, C.; Suard, E.; Fourquet, J. L.; Le Berre, F.; Crosnier-Lopez, M. P. *J. Solid State Chem.* **2009**, *182*, 317.
(28) Tassel, C.; Pruneda, J. M.; Hayashi, N.; Watanabe, T.; Kitada, A.; Tsujimoto, Y.; Kageyama, H.; Yoshimura, K.; Takano, M.; Nishi, M.; Ohoyama, K.; Mizumaki, M.; Kawamura, N.; Iniguez, J.; Canadell, E. *J. Am. Chem. Soc.* **2009**, *131*, 221.
(29) Brese, N. E.; O'Keeffe, M. *Acta Crystallogr.* **1991**, *B47*, 192.
(30) Ida, S.; Ogata, C.; Eguchi, M.; Youngblood, W. J.; Mallouk, T. E.; Matsumoto, Y. *J. Am. Chem. Soc.* **2008**, *130*, 7052.
(31) Voorhees, P. W. *J. Stat. Phys.* **1985**, *38*, 231.
(32) Zinke-Allmang, M. *Thin Solid Films* **1999**, *346*, 1.
(33) Inaguma, Y.; Liquan, C.; Itoh, M.; Nakamura, T.; Uchida, T.; Ikuta, H.; Wakihara, M. *Solid State Commun.* **1993**, *86*, 689.
(34) Thangadurai, V.; Shulka, A. K.; Gopalakrishnan, J.; Joubert, O.; Brohan, L.; Tournoux, M. *Mater. Sci. Forum* **2000**, *321*−*324*, 965.